

Computational Estimation of Resolution in Reconstruction Techniques Utilizing Sparsity, Total Variation, and Non-negativity

Keith Dillon^{a,b,*}, Yeshaiah Fainman^c, Yu-Ping Wang^{a,b}

^aDepartment of Biomedical Engineering, Tulane University, New Orleans, LA, USA

^bDepartment of Biostatistics and Bioinformatics, Tulane University, New Orleans, LA, USA

^cDepartment of Electrical and Computer Engineering, University of California at San Diego, La Jolla, CA, USA

Abstract. Techniques which exploit properties such as sparsity and total-variation have provided the ability to reconstruct images which surpass the conventional limits of imaging. This leads to difficulties in assessing the result, as conventional metrics for resolution are no longer valid. We develop a numerical approach to evaluating the second-order statistics of the estimate by relating a confidence interval on the solution to a confidence interval on a pixel value, and from this we formulate a novel approach to estimating the spatial resolution. With this estimate we can calculate the resolution at each point subject to chosen bounds on the desired precision and confidence. We demonstrate the method for limited-angle tomographic reconstructions utilizing non-negativity, sparse regularization, total-variation minimization, and their combinations. This provides a means to visualize and understand the effect on the image inherent in these penalties and constraints. Examples are provided using simulated data for different methods, and the results are shown to agree with resolution calculated empirically via the local edge response.

Keywords: Image reconstruction, resolution, convex optimization, sparsity, non-negativity, total variation.

*Keith Dillon, kdillon1@tulane.edu

1 Introduction

Imaging systems are most commonly (and intuitively) characterized by their resolution. Resolution broadly denotes the smallest spatial scale for which details may be discerned in an image, and has been examined from a variety of perspectives.¹ It is most easily estimated in practice by some variant of the Rayleigh criterion,² or via the ground-resolved distance.³ This can be made more rigorous using formulations based on decision theory and information theory.⁴ A deeper perspective is provided by signal processing theory which relates resolution to physical properties of the imaging system such as aperture size,² by viewing the resolution as a spatial-frequency cutoff.

Modern reconstruction techniques, however, can often surpass such spectral limits. The key is the use of numerical optimization algorithms which can incorporate sophisticated forms of prior knowledge. One example is non-negative least squares (NNLS),⁵ imposing physical knowledge about non-negativity of parameters like tissue density in limited-angle tomography,⁶ or light intensity in optical analogs.⁷ Another example is LASSO,⁸ which imposes the presumption of sparsity of the object. These and related approaches are widely used in Compressed Sensing.⁹⁻¹¹ A method closely related to sparsity is Total Variation (TV) minimization,¹² which enforces sparsity of edges to model images with large roughly-constant regions. TV minimization is particularly effective in medical imaging modalities such as MRI¹³ and CT¹⁴ given the small number of tissue types in a typical image.

Due to the ability to surpass convention resolution limits, such optimization-based techniques are also referred to as super-resolution¹⁵ (e.g., super-resolution using non-negativity,¹⁶ sparsity,^{17,18} or smoothness constraints¹⁹). Such approaches are extremely common in modern image processing techniques, yet can be very difficult to understand and characterize, with most results stopping with the question of solution uniqueness.²⁰⁻²² In imaging terms, this implies a cutoff for sufficient data collection²³ rather than a description of performance. In practice, algorithm performance has generally been evaluated empirically, where the trade-off between resolution and signal-to-noise may also be incorporated,^{24,25} and where improvements can be seen.²⁶

There are some interesting approaches which can extend the classical methods for calculating resolution in different ways, and potentially be extended to address the above limitation. In the geosensing

field, Backus-Gilbert theory²⁷⁻²⁹ computes a metric of the most compact estimator at each point, based on Gaussian statistics. Stark^{30,31} proposed a generalization of this theory to incorporate more general prior knowledge, though his framework still leaves open the question of how to formulate and solve the problem for particular systems. A practical approach utilizes local linearization³² of the optimization objective and notably can address Poisson noise statistics, making it quite appropriate for the low signal levels in PET systems.^{33,34} However, linearization presumes smoothness of the penalty function, making it a problematic choice for methods involving sparsity-imposing or non-negativity constraints. One may attempt to resolve such limitations by employing techniques such as by smoothing the objective,³⁵ or by employing finite differences in a brute force linearization technique³² though such ad hoc approaches need to be developed for each application. Further, it should be noted that the result of local linearization is technically an estimate of the width of the impulse response, not the reconstructed resolution.

In this paper we will pose resolution in terms of an optimization problem for finding the highest-resolution pixel possible at each point. We will incorporate prior knowledge via constraints on the posterior distribution which form confidence intervals on the image estimate. We use a novel approach based on duality theory to find a set of conditions for bounds on these constraints, which form the feasible set of our optimization problem. And unlike local linearization methods, we do not require uniqueness or smoothness (or for that matter even convexity) of the optimization objective. Our approach will quantify trade-offs between resolution, confidence intervals on the solution, and precision on the pixel value. Hence our definition of resolution will be the following:

Resolution: the spatial spread of the most compact pixel at a chosen location whose value may be estimated at a given precision and given statistical confidence.

We will develop a framework to perform this estimate with a variety of different reconstruction techniques.

2 Methods

We focus on a discrete linear system model, defined as $\mathbf{b} = \mathbf{A}\mathbf{x} + \mathbf{n}$, where \mathbf{A} is the (known) $m \times n$ system matrix; \mathbf{b} is a vector containing the measured sensor data; \mathbf{x} is a vector containing the pixels or voxels of the reconstructed image of the object; and \mathbf{n} is an unknown noise vector about which we only have statistical information. For imaging examples, see the mathematical formulations in algebraic reconstruction for CT,³⁶ and model-based reconstruction for MRI.³⁷

The MAP estimate³⁸ of \mathbf{x} is the optimal solution to the following problem,

$$p = \max_{\mathbf{x}} P(\mathbf{x}|\mathbf{b}) = \max_{\mathbf{x}} \frac{P(\mathbf{b}|\mathbf{x})P(\mathbf{x})}{P(\mathbf{b})}. \quad (1)$$

The solution, $\mathbf{x}^{(MAP)}$, is the most-probable solution out of (typically) infinite possible solutions and p gives its probability. Assuming the noise vector \mathbf{n} is zero-mean with independent variances σ_2^2 for each element, common choices for the prior distribution lead (via taking the log and rearranging constants) to the techniques of Table 1.

LMS estimation (called Tikhonov regularization³⁹) based on a Gaussian prior can be directly solved via linear algebra techniques.⁴⁰ The regularization parameter $\lambda_{LMS} = \sigma_2^2/\sigma_1^2$ results from the statistics of the noise and object, respectively. NNLS may be viewed as the result of a truncated Gaussian prior, which is separated into a conventional Gaussian prior and a non-negativity constraint. The popular techniques for imposing sparsity (which we denote with ‘‘L1R’’ for ℓ_1 -regularized) such as LASSO can be viewed as resulting from a multidimensional Laplace prior,⁴¹ where $\lambda_{L1R} = 2\frac{\sigma_2^2}{\sigma_1}$, with σ_1 as the variance of the prior. Extensions which involve non-identity covariances or transformations of \mathbf{x} to a different basis, such

Table 1 MAP estimates and corresponding problems for bounding the minimum value a pixel can take.

Case	MAP Problem	Pixel Minimum
LMS	$\alpha_{LMS} = \min_{\mathbf{x}} \ \mathbf{Ax} - \mathbf{b}\ _2^2 + \lambda \ \mathbf{x}\ _2^2$	$\min_{\mathbf{x}} \mathbf{c}^T \mathbf{x}$ $\ \mathbf{Ax} - \mathbf{b}\ _2^2 + \lambda \ \mathbf{x}\ _2^2 \leq \alpha_{LMS} + \epsilon$
NNLS	$\alpha_{NNLS} = \min_{\mathbf{x}} \ \mathbf{Ax} - \mathbf{b}\ _2^2 + \lambda_{LS} \ \mathbf{x}\ _2^2$ $\mathbf{x} \geq \mathbf{0}$.	$\min_{\mathbf{x}} \mathbf{c}^T \mathbf{x}$ $\ \mathbf{Ax} - \mathbf{b}\ _2^2 + \lambda_{LS} \ \mathbf{x}\ _2^2 \leq \alpha_{NNLS} + \epsilon$ $\mathbf{x} \geq \mathbf{0}$
L1R	$\alpha_{L1R} = \min_{\mathbf{x}} \ \mathbf{Ax} - \mathbf{b}\ _2^2 + \lambda_{L1R} \ \mathbf{I}_c \mathbf{Mx}\ _1$	$\min_{\mathbf{x}} \mathbf{c}^T \mathbf{x}$ $\ \mathbf{Ax} - \mathbf{b}\ _2^2 + \lambda_{L1R} \ \mathbf{I}_c \mathbf{Mx}\ _1 \leq \alpha_{L1R} + \epsilon$
NNL1R	$\alpha_{NNL1R} = \min_{\mathbf{x}} \ \mathbf{Ax} - \mathbf{b}\ _2^2 + \lambda_{L1R} \ \mathbf{I}_c \mathbf{Mx}\ _1$ $\mathbf{x} \geq \mathbf{0}$	$\min_{\mathbf{x}} \mathbf{c}^T \mathbf{x}$ $\ \mathbf{Ax} - \mathbf{b}\ _2^2 + \lambda_{L1R} \ \mathbf{I}_c \mathbf{Mx}\ _1 \leq \alpha_{NNL1R} + \epsilon$ $\mathbf{x} \geq \mathbf{0}$

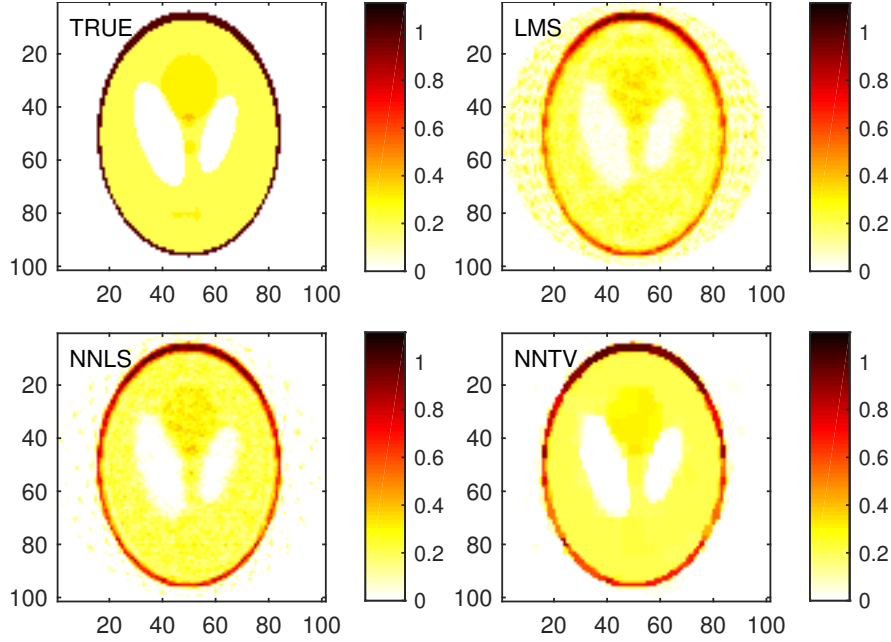


Fig 1 True Shepp-Logan⁴³ phantom used versus reconstructions of limited-angle CT simulation with a noise level chosen to achieve SNR=100:1. Least mean-squared (LMS, SNR=3.4:1), non-negative least-squares (NNLS, SNR=6.5:1), and Non-negative total-variation regularized (NNTV, SNR=7.4:1) optimization. $N = 100 \times 100$, 30 equally-spaced parallel projections.

as TV minimization,¹² or which involve complex \mathbf{x} such as for MRI,¹³ are incorporated by including a (not-necessarily square) matrix \mathbf{M} in the prior. The matrix \mathbf{I}_c allows us to address complex numbers if needed, by choosing $\mathbf{I}_c = \mathbf{I}$, the identity matrix, for the real case, and $\mathbf{I}_c = (\mathbf{I}, i\mathbf{I})$ for the complex case, with $i = \sqrt{-1}$.

In Fig. 1 we give examples of reconstruction results for a limited-view tomography⁴² simulation using 30 equally-spaced views. We compare the LMS estimate (SNR=3.4:1) to non-negative least-squares (NNLS, SNR=6.5:1) and non-negative total-variation regularized (NNTV, SNR=7.4:1) estimates. The latter employs a matrix \mathbf{M} that computes finite differences along each dimension.

Clearly the resolution differs in some sense between techniques, and we will develop a method in this paper for understanding this variation. Previously⁴⁴ we developed conditions for the existence of bounds on pixels and we extended this idea to conditions for uniqueness of the solution.^{45,46} In this paper we will extend such conditions to statistical descriptions for noise and prior knowledge in image reconstruction problems, where instead of unique solutions, we will seek solutions subject to statistical bounds on

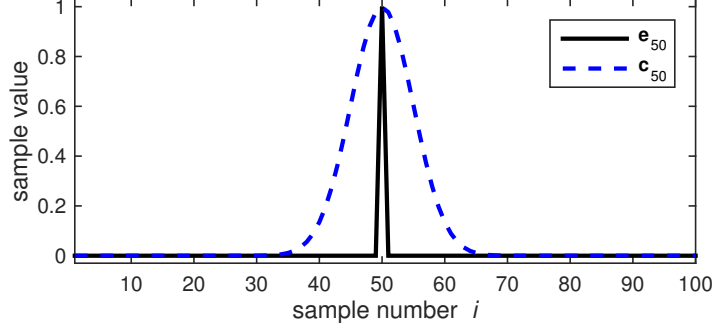


Fig 2 One-dimensional example of best-possible pixel or resolution cell \mathbf{e}_k (a vector of zeros with a one in its k^{th} element) versus lower resolution pixel \mathbf{c} for $k = 50$ with $n = 100$, normalized to have peak value of 1.0 for comparison. The sample number here gives the spatial location so we can view pixels as a distribution over position.

confidence.

The Definition of a Pixel “c”

We use a discrete formulation as done elsewhere⁴⁷ where we define “high resolution” as the base sample spacing, which we choose to be a regular grid at a spacing that is as fine or finer than the highest resolution possible (for example, the highest possible given our practical computational capabilities). A “low-resolution” pixel, which we will describe by the vector \mathbf{c} , is defined on the high-resolution grid with a distribution that has some spread over multiple pixels, hence a distribution over space. Note that we are defining a “pixel”⁴⁸ as a vector of values on the high-resolution grid, not as the sample of the object itself, which is simply a scalar estimate (Fig. 2). This follows the linear estimator in Backus-Gilbert theory, a linear functional which calculates the parameter of interest, in our case a sample value for the image of the object. In this paper we will seek the low-resolution pixel which describes the smallest region over which we can calculate the average value with a predetermined degree of confidence. The pixel value itself (i.e., the scalar estimate mentioned earlier) is $\mathbf{c}^T \mathbf{x}$.

2.1 Conditions for Precision via Duality

Now we will formulate a set of conditions to determine when we can estimate a pixel’s value to a desired precision with a chosen degree of confidence. These will be the basis for an optimization program to estimate resolution. To be clear, we have three distinct metrics of interest:

1. *Resolution: the spatial spread of the pixel \mathbf{c} about its k^{th} element,*
2. *Precision: the spread (interval) of scalar values of $\mathbf{c}^T \mathbf{x}$,*
3. *Confidence: the confidence interval on the statistical spread of $P(\mathbf{x}|\mathbf{b})$.*

In particular we will start by asking if, for a given pixel estimator \mathbf{c} and confidence (which we will denote with f), the value of $\mathbf{c}^T \mathbf{x}$ falls within a maximum allowable limit $\delta_k^{(max)}$ for the precision. This can be tested with the following equation, where we independently calculate the maximum and minimum of $\mathbf{c}^T \mathbf{x}$, and take the difference,

$$\max_{\mathbf{x}} \mathbf{c}^T \mathbf{x} - \min_{\mathbf{x}} \mathbf{c}^T \mathbf{x} \leq \delta_k^{(max)}. \quad (2)$$

$P(\mathbf{x}|\mathbf{b}) \geq f P(\mathbf{x}^{(MAP)}|\mathbf{b}) \quad P(\mathbf{x}|\mathbf{b}) \geq f P(\mathbf{x}^{(MAP)}|\mathbf{b})$

We imposed a chance constraint⁴⁹ on the MAP solution, which sets a threshold for robustness of the estimate. The parameter $f \in (0, 1)$ is a fraction chosen to adjust the desired confidence threshold, which leads to a relaxation of the range of $\mathbf{c}^T \mathbf{x}$ around the optimal. This gives a constraint on the statistical spread of the posterior distribution, analogous to a constraint on the variance. Hence the constraint forces us to seek a

more robust estimate at some lower resolution. As defined, $f = 1$ implies minimum confidence while $f = 0$ implies maximum confidence. For a Gaussian distribution, $f = 0.6$ constrains the confidence interval to be the variance. Taking the log similar to MAP estimation, we get the optimization problems in Table 1 for the minimums (the maximums are similar with minimization replaced by maximization). The parameter ϵ in Table 1 relates to the confidence parameter f as

$$\epsilon = -2\sigma_2^2 \log f. \quad (3)$$

Each of these problems can be formulated as a second-order cone program (SOCP).⁵⁰ SOCP's are convex and hence have an optimum that, if it exists, is guaranteed to be global. Further, SOCP's can be solved efficiently with a variety of free and commercial software tools.⁵¹⁻⁵³

We can replace the optimization test of Eq. (2) with a direct set of conditions using duality theory. A dual problem can be viewed as a test of the optimality conditions of a (primal) optimization problem, giving a bound on the optimal. The duals of the minimization bound problems of Table 1, as well as of their maximization counterparts, are given in Table 2. The dual optimization problems provide bounds on

Table 2 Dual optimization problems for bounding the values a pixel can take.

Case	Dual of Minimum	Dual of Maximum
LMS	$\max_{\mathbf{y}, \mathbf{z}, \mu} -\mathbf{b}^T \mathbf{y} - \mu \sqrt{\alpha_{LMS} + \epsilon}$ $\mathbf{A}^T \mathbf{y} + \mathbf{c} + \sqrt{\lambda_{LS}} \mathbf{z} = \mathbf{0}$ $\sqrt{\ \mathbf{y}\ _2^2 + \ \mathbf{z}\ _2^2} \leq \mu.$	$\max_{\mathbf{y}, \mathbf{z}, \mu} -\mathbf{b}^T \mathbf{y} - \mu \sqrt{\alpha_{LMS} + \epsilon}$ $\mathbf{A}^T \mathbf{y} - \mathbf{c} + \sqrt{\lambda_{LS}} \mathbf{z} = \mathbf{0}$ $\sqrt{\ \mathbf{y}\ _2^2 + \ \mathbf{z}\ _2^2} \leq \mu.$
NNLS	$\max_{\mathbf{y}, \mathbf{z}, \mu} -\mathbf{b}^T \mathbf{y} - \mu \sqrt{\alpha_{NNLS} + \epsilon}$ $\mathbf{A}^T \mathbf{y} + \mathbf{c} + \sqrt{\lambda_{LS}} \mathbf{z} \geq \mathbf{0}$ $\sqrt{\ \mathbf{y}\ _2^2 + \ \mathbf{z}\ _2^2} \leq \mu.$	$\max_{\mathbf{y}, \mathbf{z}, \mu} -\mathbf{b}^T \mathbf{y} - \mu \sqrt{\alpha_{NNLS} + \epsilon}$ $\mathbf{A}^T \mathbf{y} - \mathbf{c} + \sqrt{\lambda_{LS}} \mathbf{z} \geq \mathbf{0}$ $\sqrt{\ \mathbf{y}\ _2^2 + \ \mathbf{z}\ _2^2} \leq \mu.$
L1R	$\max_{\mathbf{y}, \mathbf{u}, \mu, \eta} -\mathbf{b}^T \mathbf{y} - \mu(\alpha_{L1R} + \epsilon) - \eta$ $\mathbf{A}^T \mathbf{y} + \mathbf{c} + \mathbf{M}^T \mathbf{u} = \mathbf{0}$ $\ \mathbf{I}_c \mathbf{u}\ _\infty \leq \mu \lambda_{L1R}$ $\ \mathbf{y}\ _2^2 \leq 4\eta\mu$	$\max_{\mathbf{y}, \mathbf{u}, \mu, \eta} -\mathbf{b}^T \mathbf{y} - \mu(\alpha_{L1R} + \epsilon) - \eta$ $\mathbf{A}^T \mathbf{y} - \mathbf{c} + \mathbf{M}^T \mathbf{u} = \mathbf{0}$ $\ \mathbf{I}_c \mathbf{u}\ _\infty \leq \mu \lambda_{L1R}$ $\ \mathbf{y}\ _2^2 \leq 4\eta\mu$
NNL1R	$\max_{\mathbf{y}, \mathbf{u}, \mu, \eta} -\mathbf{b}^T \mathbf{y} - \mu(\alpha_{L1R} + \epsilon) - \eta$ $\mathbf{A}^T \mathbf{y} + \mathbf{c} + \mathbf{M}^T \mathbf{u} \geq \mathbf{0}$ $\ \mathbf{I}_c \mathbf{u}\ _\infty \leq \mu \lambda_{L1R}$ $\ \mathbf{y}\ _2^2 \leq 4\eta\mu$	$\max_{\mathbf{y}, \mathbf{u}, \mu, \eta} -\mathbf{b}^T \mathbf{y} - \mu(\alpha_{L1R} + \epsilon) - \eta$ $\mathbf{A}^T \mathbf{y} - \mathbf{c} + \mathbf{M}^T \mathbf{u} \geq \mathbf{0}$ $\ \mathbf{I}_c \mathbf{u}\ _\infty \leq \mu \lambda_{L1R}$ $\ \mathbf{y}\ _2^2 \leq 4\eta\mu$

the primal problems. Hence by testing if a dual feasible point exists for the dual minimization and dual maximization that achieves a certain objective, we can test if the respective primal problem is bounded by this value. By simultaneously testing if a dual feasible solution exists for both the maximum and minimum simultaneously, subject to the constraint that their optimal are bounded by our desired precision constraint, we can prove or disprove whether the primal problems are bounded by this constraint. This gives us a set of conditions. In Table 3, we give such conditions for each case.

2.2 Resolution Estimation Program

Our goal in this section will be to determine the most concentrated pixel \mathbf{c} which fulfills the conditions of Table 3, for a choice of precision and confidence. We define the metric for concentration of \mathbf{c} as the spatial variance, which we estimate with the following general formulation,

$$\mathbf{c}^* = \arg \min_{\mathbf{c}, \text{dual vars}} \mathbf{w}^T \mathbf{c}$$

$$\mathbf{c}^T \mathbf{x} \text{ fulfills our conditions (Table 3.)} \quad (4)$$

$$\mathbf{c} \geq \mathbf{0}$$

$$\mathbf{1}^T \mathbf{c} = 1.$$

Table 3 Conditions for Desired Precision, confidence, and pixel.

Case	Conditions	Dual Variables
LMS	$\mathbf{b}^T \mathbf{y} + \mu \sqrt{\alpha_{LMS} + \epsilon} + \mathbf{b}^T \mathbf{y}' + \mu' \sqrt{\alpha_{LMS} + \epsilon} \leq \delta_k^{(max)}$ $\mathbf{A}^T \mathbf{y} - \mathbf{c} + \sqrt{\lambda_{LS}} \mathbf{z} = \mathbf{0}$ $\mathbf{A}^T \mathbf{y}' + \mathbf{c} + \sqrt{\lambda_{LS}} \mathbf{z}' = \mathbf{0}$ $\sqrt{\ \mathbf{y}\ _2^2 + \ \mathbf{z}\ _2^2} \leq \mu$ $\sqrt{\ \mathbf{y}'\ _2^2 + \ \mathbf{z}'\ _2^2} \leq \mu'$	$\mathbf{y}, \mathbf{z}, \mu,$ $\mathbf{y}', \mathbf{z}', \mu'$
NNLS	$\mathbf{b}^T \mathbf{y} + \mu \sqrt{\alpha_{NNLS} + \epsilon} + \mathbf{b}^T \mathbf{y}' + \mu' \sqrt{\alpha_{NNLS} + \epsilon} \leq \delta_k^{(max)}$ $\mathbf{A}^T \mathbf{y} - \mathbf{c} + \sqrt{\lambda_{LS}} \mathbf{z} \geq \mathbf{0}$ $\mathbf{A}^T \mathbf{y}' + \mathbf{c} + \sqrt{\lambda_{LS}} \mathbf{z}' \geq \mathbf{0}$ $\sqrt{\ \mathbf{y}\ _2^2 + \ \mathbf{z}\ _2^2} \leq \mu$ $\sqrt{\ \mathbf{y}'\ _2^2 + \ \mathbf{z}'\ _2^2} \leq \mu'$	$\mathbf{y}, \mathbf{z}, \mu,$ $\mathbf{y}', \mathbf{z}', \mu'$
L1R	$\mathbf{b}^T \mathbf{y} + \mu(\alpha_{L1R} + \epsilon) + \eta + \mathbf{b}^T \mathbf{y}' + \mu'(\alpha_{L1R} + \epsilon) + \eta' \leq \delta_k^{(max)}$ $\mathbf{A}^T \mathbf{y} - \mathbf{c} + \mathbf{M}^T \mathbf{u} = \mathbf{0}$ $\mathbf{A}^T \mathbf{y}' + \mathbf{c} + \mathbf{M}^T \mathbf{u}' = \mathbf{0}$ $\ \mathbf{I}_c \mathbf{u}\ _\infty \leq \mu \lambda_{L1R}$ $\ \mathbf{I}_c \mathbf{u}'\ _\infty \leq \mu' \lambda_{L1R}$ $\ \mathbf{y}\ _2^2 \leq 4\eta\mu$ $\ \mathbf{y}'\ _2^2 \leq 4\eta'\mu'$	$\mathbf{y}, \mathbf{u}, \mu, \eta,$ $\mathbf{y}', \mathbf{u}', \mu', \eta'$
NNL1R	$\mathbf{b}^T \mathbf{y} + \mu(\alpha_{NNL1R} + \epsilon) + \eta + \mathbf{b}^T \mathbf{y}' + \mu'(\alpha_{NNL1R} + \epsilon) + \eta' \leq \delta_k^{(max)}$ $\mathbf{A}^T \mathbf{y} - \mathbf{c} + \mathbf{M}^T \mathbf{u} \geq \mathbf{0}$ $\mathbf{A}^T \mathbf{y}' + \mathbf{c} + \mathbf{M}^T \mathbf{u}' \geq \mathbf{0}$ $\ \mathbf{I}_c \mathbf{u}\ _\infty \leq \mu \lambda_{L1R}$ $\ \mathbf{I}_c \mathbf{u}'\ _\infty \leq \mu' \lambda_{L1R}$ $\ \mathbf{y}\ _2^2 \leq 4\eta\mu$ $\ \mathbf{y}'\ _2^2 \leq 4\eta'\mu'$	$\mathbf{y}, \mathbf{u}, \mu, \eta,$ $\mathbf{y}', \mathbf{u}', \mu', \eta'$

The notation $\mathbf{0}$ and $\mathbf{1}$ denote vectors of zeros and ones respectively. The constraints $\mathbf{c} \geq \mathbf{0}$ and $\mathbf{1}^T \mathbf{c} = 1$ enforce the notion of the low-resolution pixel as a distribution (i.e., positivity and unit sum). The vector \mathbf{w} is similar to that of Backus-Gilbert theory, as a weighting which varies quadratically with distance from the point of interest, to approximate an estimate of variance. The constraint “ $\mathbf{c}^T \mathbf{x}$ fulfills our conditions” refers to the appropriate conditions from Table 3 for the reconstruction technique we are using. The optimization is performed over the dual variables in Table 3 along with \mathbf{c} . As the conditions in Table 3 form convex constraints (as per convex optimization theory), and the objective and additional constraints in Eq. (4) are linear, this is always a convex optimization problem. The LMS case yields a version of the Backus-Gilbert estimate.

For the NNLS case, for example, we get the following convex optimization problem

$$\begin{aligned}
 \mathbf{c}^* = \arg \min_{\mathbf{c}, \mathbf{y}, \mathbf{z}, \mu, \mathbf{y}', \mathbf{z}', \mu'} & \mathbf{w}^T \mathbf{c} \\
 \mathbf{b}^T \mathbf{y} + \mu \sqrt{\alpha_{NNLS} + \epsilon} + \mathbf{b}^T \mathbf{y}' + \mu' \sqrt{\alpha_{NNLS} + \epsilon} & \leq \delta_k^{(max)} \\
 \mathbf{A}^T \mathbf{y} - \mathbf{c} + \sqrt{\lambda_{LS}} \mathbf{z} & \geq \mathbf{0} \\
 \mathbf{A}^T \mathbf{y}' + \mathbf{c} + \sqrt{\lambda_{LS}} \mathbf{z}' & \geq \mathbf{0} \\
 \sqrt{\|\mathbf{y}\|_2^2 + \|\mathbf{z}\|_2^2} & \leq \mu \\
 \sqrt{\|\mathbf{y}'\|_2^2 + \|\mathbf{z}'\|_2^2} & \leq \mu' \\
 \mathbf{c} & \geq \mathbf{0} \\
 \mathbf{1}^T \mathbf{c} & = 1.
 \end{aligned} \tag{5}$$

Note that this optimization problem must be solved for each point (by forming a weighting \mathbf{w} concentrated there) if the resolution is spatially-varying, which we expect it to be in general. This pixel-wise estimation would also be required of the Backus-Gilbert and local linearization techniques. To find the range of pixel values for each \mathbf{c}^* we can use the optimization problems of Table 1, or simply compute $\mathbf{c}^{*T} \mathbf{x}$, using any

feasible \mathbf{x} , such as the MAP solution, to get an estimate within the set precision constraint.

The statistical parameters for the likelihood and prior (leading to a choice for the corresponding λ) may be estimated from the system or data itself. A suggested choice for the precision $\delta_k^{(max)}$ is some small value corresponding to the best dynamic range that can be expected; we used 0.01 for signals that range within $[0, 1]$ as it is comparable to the SNR of the system. And finally ϵ results from the noise statistic and the choice of f , which should be set relatively high to model the posterior effectively; a value of 0.9 worked well for the cases we tested. We determined this choice by matching the Backus-Gilbert estimate to a theoretical estimate based on considering the spectral cutoff for the system.

Examples of the \mathbf{c} computed from each case for two different locations are provided in Fig. 3 for our phantom simulation. The resolution of the system at this point is the spread of these distributions. We can

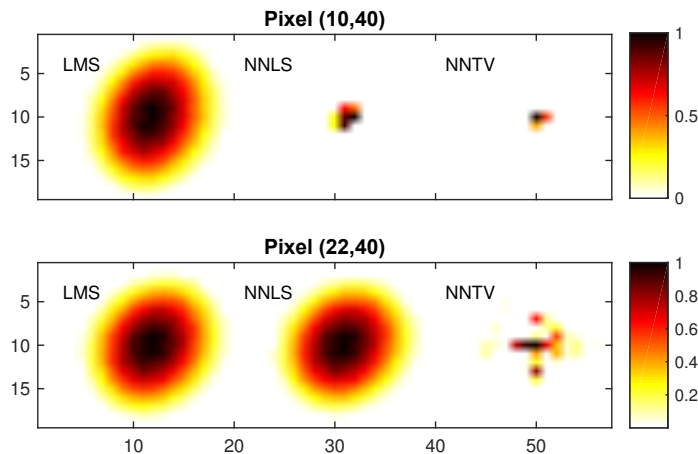


Fig 3 Pixels (\mathbf{c}) for different prior knowledge assumptions for location (row,col)=(10,40) (top row), and (row,col)=(22,40) (bottom row), at $f = 0.9$ and $\delta_k^{(max)} = 0.1$, $N = 100 \times 100$, 50 parallel projections. Peaks normalized to 1.0. Axes are provided only to demonstrate size, not absolute locations.

see that the ranking in pixel concentration roughly matches the subjective expectation we had from Fig. 1. In Fig. 4 we give the resolution estimated at every pixel for these cases with the same confidence and precision requirements, as the standard deviations of \mathbf{c} about the point of interest.

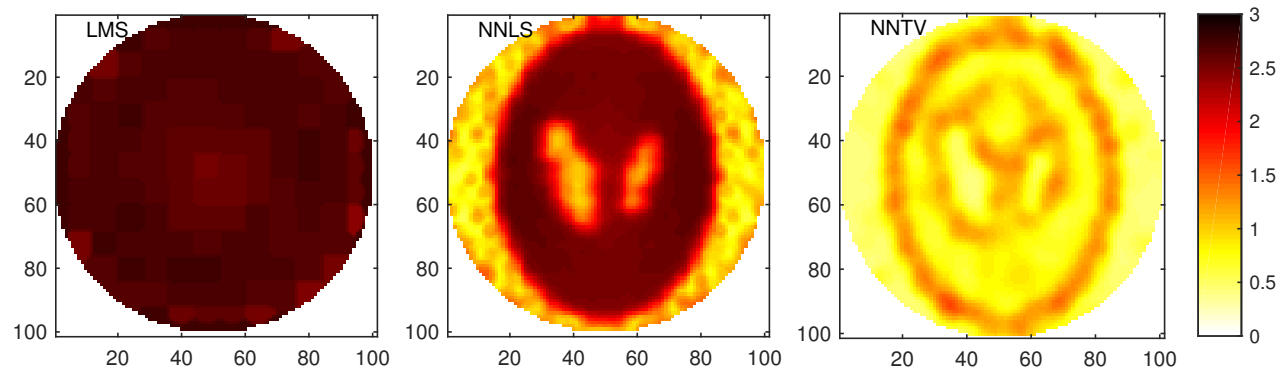


Fig 4 Resolution at each point in image measured by standard deviation (STD) in units of pixels at $f = 0.9$ and $\delta_k^{(max)} = 0.1$, $N = 100$, 30 parallel projections. Higher values imply worse resolution (more spread out pixel).

We see some interesting structure in the resolution estimates, both between techniques and within the image. The LMS result was roughly constant, increasing slightly away from the center, due to the properties of the tomographic system. The non-negativity constraint resulted in improved resolution for the NNLS

case, especially for the regions where the phantom was zero, but degraded to nearly the LMS values in large regions where we see the estimate of Fig. 4 also looks correspondingly poor. The NNTV result was overall very good with a limited loss of resolution at edges.

2.3 Validation

For comparison, we generated a large number of realizations of the MAP estimates from Fig. 1 to estimate the pixel statistics. We generated 5000 realizations of the noisy data (again with SNR 100:1) and computed the sample variance of the reconstructed images for the three techniques. In Fig. 5 we show the standard deviations of each pixel for the three methods. We can see qualitative agreement with our resolution estimates; the LMS estimate is generally uniform, whereas the NNLS and NNTV are more variable for nonzero and edge pixels, respectively. Pixel values have lower confidence if the variance is high, hence a reduction in resolution at these high-variance regions is needed to maintain the confidence constraint there.

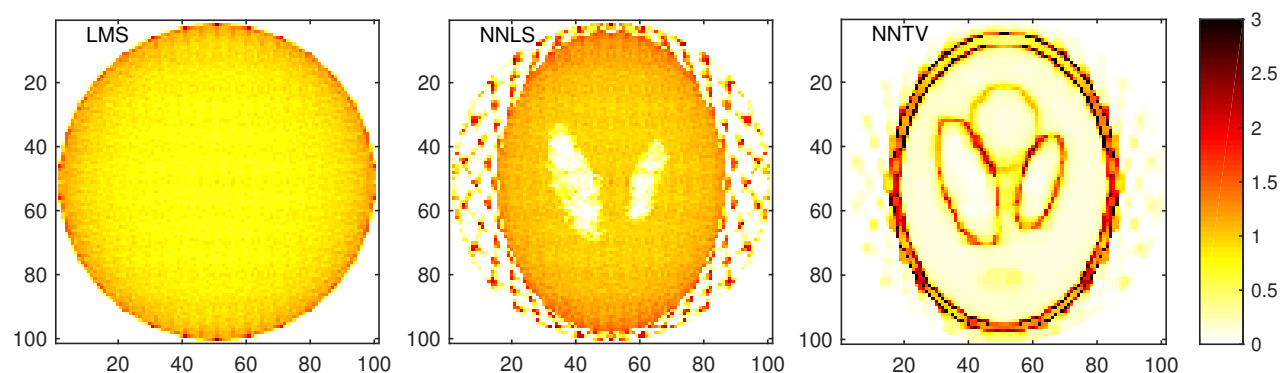


Fig 5 Standard deviation of each pixel for MAP estimates, calculated using 5000 realizations with SNR 100:1

For an additional form of validation, we used the expected mean image (the mean pixel values over all realizations) to calculate expected edge responses, similar to techniques that estimate the expected value of the impulse response.³² The edge response or edge profile⁵⁴ provides an intuitive approach for estimating the resolution directly from the image, and is popular in super-resolution algorithms.⁵⁵ This requires us to carefully choose the location of edges in the image, and have reasonably well-isolated examples. We performed the comparison using the edge responses rather than the impulse response, because the derivative of the sample mean is still fairly noisy. So we took the integral of our low-resolution pixel estimates, making a model of the predicted edge at various locations, to compare directly to the edges. Comparisons are given in Fig. 6 where we overlay the edge models for three locations over the mean image estimate. We see that the edge models fit quite well for the well-isolated edges at pixels 18 and 42. The apparent high-resolution of the edge at pixel 68 is likely an artifact of the image structure, given that it appears higher-resolution even for the LMS case.

3 Discussion

In this paper we developed an optimization-based method for computing a form of second order statistics of MAP solutions, which we related to the classical idea of resolution. Convex optimization remains something of an “art”,⁵⁶ where non-obvious manipulations of the problem can often convert a very difficult numerical optimization problem into a simple one. Hence we provided multiple general formulations to compute resolution for a variety of important reconstruction techniques, all of which are straightforward to solve with off the shelf second-order cone program (SOCP) solvers.

The resolution calculated by our method incorporates the trade-offs that results from incorporating prior knowledge. The examples demonstrated agreement with the intuitive expectation that resolution should be

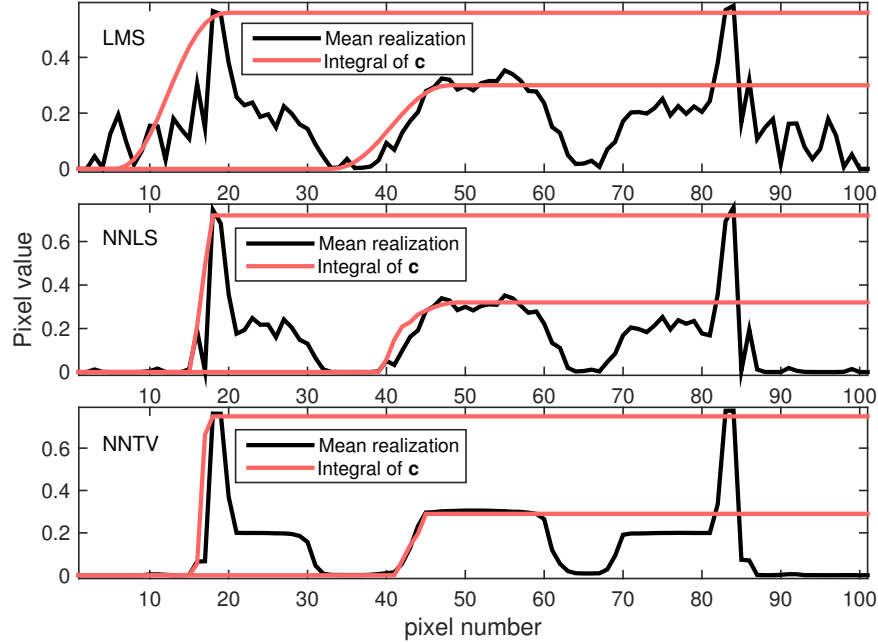


Fig 6 Edge models for low-resolution pixels centered at 18, 42, and 68, versus mean estimated image for row 40 using LMS, NNLS, and NNTV techniques, showing good agreement with the optimization-based method proposed in this paper. Edge models are formed by integrating low-resolution pixel estimate (c from Eq. (4)) and scaling to similar height as the image.

improved by prior knowledge (as seen in the improved resolution in the other cases over the LMS estimate), and indeed that resolution was better in regions of the images where the prior knowledge was more pertinent; in the NNLS method, resolution was better in and near regions that were closer to zero, whereas in NNTV resolution was also improved in regions with less edges. Our results should also be useful for determining the best choice of prior to use. If a choice of prior results in a solution which is very sensitive to noise, our technique will quantify this sensitivity. For example, with the NNTV method, the MAP solution in Fig. 1 has sharp edges which may be misleading; small amounts of noise result in small variations of the location of these sharp edges (hence the high variance at the edges in Fig. 5). Our resolution estimate captures this without the need to collect multiple realizations of the image.

In order to calculate the spatial details of the resolution, it must be calculated at a range of points across the image. Ideally, the calculation could be done at every pixel, though this may be very challenging for large images. It can also be calculated at a reduced or adaptive sample spacing, such as only on a line or lower-resolution grid, or only at a region of interest such as a potential lesion. This load can also be alleviated by parallelization since the calculation for each pixel is independent of others; the two-dimensional results shown here calculated on a parallel computing system with 360 dedicated cores, taking a total of between 40 and 80 minutes for the methods.

3.1 Acknowledgments

The authors wish to thank the NIH(R01GM109068, R01MH104680, R01MH107354), and NSF (1539067) for support.

References

- 1 A. J. den Dekker and A. van den Bos, "Resolution: a survey," *Journal of the Optical Society of America A* **14**, 547 (1997).
- 2 J. W. Goodman, *Introduction to Fourier Optics*, Roberts and Company Publishers (2005).

- 3 J. B. Campbell and R. H. Wynne, *Introduction to Remote Sensing*, Guilford Press (2011).
- 4 S. Van Aert, D. Van Dyck, and A. J. den Dekker, "Resolution of coherent and incoherent imaging systems reconsidered - Classical criteria and a statistical alternative," *Optics Express* **14**(9), 3830 (2006).
- 5 C. Lawson and R. Hanson, *Solving Least Squares Problems*, Classics in Applied Mathematics, Society for Industrial and Applied Mathematics (1995).
- 6 D. Verhoeven, "Limited-data computed tomography algorithms for the physical sciences," *Applied Optics* **32**, 3736 (1993).
- 7 K. Dillon and Y. Fainman, "Depth sectioning of attenuation," *Journal of the Optical Society of America A* **27**, 1347–1354 (2010).
- 8 R. J. Tibshirani, "The lasso problem and uniqueness," *Electronic Journal of Statistics* **7**, 1456–1490 (2013).
- 9 R. M. Willett, R. F. Marcia, and J. M. Nichols, "Compressed sensing for practical optical imaging systems: a tutorial," *Optical Engineering* **50**(7), 072601–072601–13 (2011).
- 10 D. J. Brady, A. Mrozack, K. MacCabe, and P. Llull, "Compressive tomography," *Advances in Optics and Photonics* **7**, 756 (2015).
- 11 O. N. Jaspán, R. Fleysher, and M. L. Lipton, "Compressed sensing MRI: a review of the clinical literature," *The British Journal of Radiology* **88**, 20150487 (2015).
- 12 L. I. Rudin, S. Osher, and E. Fatemi, "Nonlinear total variation based noise removal algorithms," *Physica D: Nonlinear Phenomena* **60**, 259–268 (1992).
- 13 M. Lustig, D. Donoho, J. Santos, and J. Pauly, "Compressed Sensing MRI," *IEEE Signal Processing Magazine* **25**, 72–82 (2008).
- 14 E. Y. Sidky and X. Pan, "Image reconstruction in circular cone-beam computed tomography by constrained, total-variation minimization," *Physics in Medicine and Biology* **53**, 4777 (2008).
- 15 H. Greenspan, "Super-Resolution in Medical Imaging," *The Computer Journal* **52**, 43–63 (2009).
- 16 D. Capel and A. Zisserman, "Super-resolution from multiple views using learnt image models," in *Proceedings of the 2001 IEEE Computer Society Conference on Computer Vision and Pattern Recognition, 2001. CVPR 2001*, **2**, II–627–II–634 vol.2 (2001).
- 17 J. Yang, J. Wright, T. Huang, and Y. Ma, "Image Super-Resolution Via Sparse Representation," *IEEE Transactions on Image Processing* **19**(11), 2861–2873 (2010).
- 18 D. L. Donoho, "Superresolution via Sparsity Constraints," *SIAM Journal on Mathematical Analysis* **23**, 1309–1331 (1992).
- 19 S. Baker and T. Kanade, "Limits on super-resolution and how to break them," *IEEE Transactions on Pattern Analysis and Machine Intelligence* **24**(9), 1167–1183 (2002).
- 20 E. J. Candès, "The restricted isometry property and its implications for compressed sensing," *Comptes Rendus Mathématique* **346**, 589–592 (2008).
- 21 D. L. Donoho and M. Elad, "Optimally sparse representation in general (nonorthogonal) dictionaries via ℓ^1 minimization," *Proceedings of the National Academy of Sciences* **100**, 2197–2202 (2003).
- 22 D. L. Donoho and J. Tanner, "Neighborliness of randomly projected simplices in high dimensions," *Proceedings of the National Academy of Sciences of the United States of America* **102**, 9452–9457 (2005).
- 23 J. S. Jørgensen and E. Y. Sidky, "How little data is enough? Phase-diagram analysis of sparsity-regularized X-ray computed tomography," *Phil. Trans. R. Soc. A* **373**, 20140387 (2015).
- 24 J. D. Evans, D. G. Polite, B. R. Whiting, J. A. OSullivan, and J. F. Williamson, "Noise-resolution tradeoffs in x-ray CT imaging: A comparison of penalized alternating minimization and filtered back-projection algorithms," *Medical Physics* **38**, 1444–1458 (2011).

- 25 S. C. Kale, X. J. Chen, and R. M. Henkelman, “Trading off SNR and resolution in MR images,” *NMR in Biomedicine* **22**, 488–494 (2009).
- 26 E. Plenge, D. H. J. Poot, M. Bernsen, G. Kotek, G. Houston, P. Wielopolski, L. van der Weerd, W. J. Niessen, and E. Meijering, “Super-resolution methods in MRI: Can they improve the trade-off between resolution, signal-to-noise ratio, and acquisition time?,” *Magnetic Resonance in Medicine* **68**, 1983–1993 (2012).
- 27 G. E. Backus and J. F. Gilbert, “Numerical Applications of a Formalism for Geophysical Inverse Problems,” *Geophysical Journal of the Royal Astronomical Society* **13**, 247–276 (1967).
- 28 G. Backus and F. Gilbert, “The Resolving Power of Gross Earth Data,” *Geophysical Journal of the Royal Astronomical Society* **16**(2), 169–205 (1968).
- 29 G. Backus, “Inference from Inadequate and Inaccurate Data, I*,” *Proceedings of the National Academy of Sciences of the United States of America* **65**, 1–7 (1970).
- 30 P. B. Stark, “Generalizing resolution,” *Inverse Problems* **24**, 034014 (2008).
- 31 S. N. Evans and P. B. Stark, “Inverse problems as statistics,” *Inverse Problems* **18**, R55 (2002).
- 32 J. Fessler and W. Rogers, “Spatial resolution properties of penalized-likelihood image reconstruction: space-invariant tomographs,” *IEEE Transactions on Image Processing* **5**, 1346–1358 (1996).
- 33 J. Qi and R. Leahy, “Resolution and noise properties of MAP reconstruction for fully 3-D PET,” *IEEE Transactions on Medical Imaging* **19**, 493–506 (2000).
- 34 S. Ahn and R. Leahy, “Analysis of Resolution and Noise Properties of Nonquadratically Regularized Image Reconstruction Methods for PET,” *IEEE Transactions on Medical Imaging* **27**, 413–424 (2008).
- 35 J. P. Haldar, V. J. Wedeen, M. Nezamzadeh, G. Dai, M. W. Weiner, N. Schuff, and Z.-P. Liang, “Improved diffusion imaging through SNR-enhancing joint reconstruction,” *Magnetic Resonance in Medicine* **69**, 277–289 (2013).
- 36 A. Andersen, “Algebraic reconstruction in CT from limited views,” *IEEE Transactions on Medical Imaging* **8**, 50–55 (1989).
- 37 J. Fessler, “Model-Based Image Reconstruction for MRI,” *IEEE Signal Processing Magazine* **27**, 81–89 (2010).
- 38 S. M. Kay, *Fundamentals of Statistical Signal Processing: Estimation Theory*, Prentice-Hall PTR (1998).
- 39 A. N. Tikhonov, A. Goncharsky, V. V. Stepanov, and A. G. Yagola, *Numerical Methods for the Solution of Ill-Posed Problems*, Springer Science & Business Media (2013).
- 40 C. L. Lawson and R. J. Hanson, *Solving Least Squares Problems*, Society for Industrial and Applied Mathematics (1987).
- 41 S. Kotz, T. Kozubowski, and K. Podgorski, *The Laplace Distribution and Generalizations: A Revisit With Applications to Communications, Economics, Engineering, and Finance*, Springer (2001).
- 42 Y.-M. Zhu, “Extrapolation method to obtain a full projection from a limited one for limited-view tomography problems,” *Medical and Biological Engineering and Computing* **31**, 323–324 (1993).
- 43 L. Shepp and B. Logan, “The Fourier reconstruction of a head section,” *IEEE Transactions on Nuclear Science* **21**(3), 21–43 (1974).
- 44 K. Dillon and Y. Fainman, “Bounding pixels in computational imaging,” *Applied Optics* **52**, D55–D63 (2013).
- 45 K. Dillon and Y. Fainman, “Element-wise uniqueness, prior knowledge, and data-dependent resolution,” *Signal, Image and Video Processing* , 1–8 (2016).
- 46 K. Dillon and Y.-P. Wang, “Imposing uniqueness to achieve sparsity,” *Signal Processing* **123**, 1–8 (2016).

- 47 E. J. Candès and C. Fernandez-Granda, “Towards a Mathematical Theory of Super-resolution,” *Communications on Pure and Applied Mathematics* (2013).
- 48 J. Blinn, “What is a pixel?,” *IEEE Computer Graphics and Applications* **25**(5), 82–87 (2005).
- 49 A. Nemirovski and A. Shapiro, “Convex Approximations of Chance Constrained Programs,” *SIAM Journal on Optimization* **17**, 969–996 (2007).
- 50 F. Alizadeh and D. Goldfarb, “Second-order cone programming,” *Mathematical Programming* **95**, 3–51 (2003).
- 51 M. Grant and S. Boyd, “CVX: Matlab Software for Disciplined Convex Programming,” (2012).
- 52 Gurobi Optimization, Inc., “Gurobi optimizer reference manual,” URL: <http://www.gurobi.com> (2012).
- 53 J. F. Sturm, “Using SeDuMi 1.02, a MATLAB toolbox for optimization over symmetric cones,” *Optimization methods and software* **11**(1-4), 625–653 (1999).
- 54 A. Rosenfeld and A. C. Kak, *Digital picture processing*, Academic Press (1982).
- 55 M.-C. Chiang and T. Boulton, “Local blur estimation and super-resolution,” in , *1997 IEEE Computer Society Conference on Computer Vision and Pattern Recognition, 1997. Proceedings*, 821–826 (1997).
- 56 S. P. Boyd and L. Vandenberghe, *Convex Optimization*, Cambridge University Press (2004).